Scaling of waiting time distribution in northern Chile

Cristián E. Siegel[1], Patricio A. Toledo[3], Raúl Madariaga[1,2], Jaime Campos[1,3]

[1]Departamento de Geofísica, Facultad de Ciencias Físicas y Matemáticas, Universidad de Chile, Blanco Encalada 2002, Santiago, Chile

[2]Laboratoire de Géologie, Ecole Normale Superieure, PSL University, 75005 Paris, France.

[3]Programa de Riesgo Sísmico PRS, Universidad de Chile, Blanco Encalada 2002, Santiago, Chile

Key Words:

- Seismicity and tectonics
- Statistical seismology
- Fractals and multifractals
- Probability distributions
- Spatial analysis
- South America

Corresponding author: Patricio A. Toledo, patoledo@ing.uchile.cl

SUMMARY

In this study, we compare the scaling of waiting time distributions in Northern Chile Subduction context. For this, we analize 7-yr high spatial resolution and low completeness magnitude IPOC seismic catalog and 45-yr USGS catalog. A unified moment-epicentral area linear dimension-time scaling relation is empirically evaluated by calculating waiting times for different ranges of magnitude and epicentral area linear dimension and estimating associated scaling coefficients, β analog to b-value and γ, the correlation fractal dimension. We find a scaling function that can be characterized with 3 distinct regions, regions whose behaviour depend on whether seismicity is in the coastal area or from intermediate depth. Moreover, high resolution localizations from IPOC catalog allows us to further observe differences in coastal seismicity, with lower plane seismicity behaviour alike intermediate depth. Thus, waiting time distribution primarily depends on whether seismicity is associated with subduction interface interaction or not, having respectively high/low correlated behaviour in the short scale region, non-exponential/exponential decay in the transition middle region and in all cases long-term clustering with a slower than exponential decay in the long scale.

1 INTRODUCTION

Earthquakes are a recurring phenomenon in the Earth's lithosphere. Regardless of the seismically active zone where an earthquake has been observed, it is to be expected that after some waiting time τ another earthquake will be observed there.

Quantifying waiting time probability distribution D is an important step towards hazard estimation. A way to do this is by exploiting D distribution similarity properties with seismic moment M, or with earthquake size S as initially proposed by Christensen et al. (2002); Corral (2003), and with epicentral area linear dimension L. Then, it follows:

$$D \propto M^{-\beta} L^{\gamma} \Psi(cM^{-\beta} L^{\gamma} \tau), \tag{1}$$

where Ψ is a scaling function, c is a constant and β, γ are scaling exponents. β is related to the seismic moment power-law distribution and γ to the epicenter power-law (fractal) spatial distribution. This is a particular case of incomplete similarity in the governing parameters M and L through a power-law scaling (Barenblatt, 2003). This relation

produces a collapse of different waiting time probability distributions given different seismic moment and epicentral area linear dimension to a common scaling function Ψ, and it was named Unified Scaling Relation for Earthquakes (USLE) (Christensen et al., 2002). The latter approach succeeded in visualizing the similarity of seismicity temporal distribution, and derived applications followed (e.g. Baiesi and Paczuski (2004); Zaliapin et al. (2008)), but there is still space to explore consequences for seismic hazard and to acknowledged the dependence of the scaling with tectonic context. Although the latter aspect was not at first considered, Davidsen and Goltz (2004); Corral (2004) found different scaling functions in seismic catalogs corresponding to different tectonic zones.

Here we explore the hypothesis that differences in the distribution of waiting times can be observed within the same subduction zone, say between interface seismicity and intermediate-depth seismicity. The importance of this lies in the fact that earthquakes coming from these sources have different potential hazard, evidenced by higher ground accelerations in intermediate depth earthquakes caused by higher stress drops or by source location, compared to interface earthquakes, particularly demonstrated in Chile in the last 30 years (Kausel & Campos, 1992; Astroza et al., 2005; Leyton et al., 2009; Derode & Campos, 2019; Otarola et al., 2021).

Northern Chile is a seismically active region suitable for testing this hypothesis, having high seismicity rates and a seismological network that allows studying statistical properties of seismicity. We use the catalog published by (Sippl et al., 2018b) that exploited the IPOC seismic network (GFZ German Research Centre For Geosciences & Institut Des Sciences De L'Univers-Centre National De La Recherche CNRS-INSU, 2006) records, and also USGS catalog compiled by Poulos et al. (2018). By first formulating the unified scaling law and second evaluating it on the catalogs we show that: (1) the scaling function is not universal and depends on whether the seismicity is associated with interface or intraplate contexts; (2) scaling exponents also differ and; (3) waiting time probability distribution D in the long scales possesses power-law decay, implying long-term correlations.

As we use two seismic catalogs with different A important consequence of this findings is that hazard estimation depends on seismic network and analysis capabilities to accurately discern the seismic events locations inside the subduction context.

We start in the next section formalizing the dimensional analysis approach to seismicity analysis, specifying hypotheses commonly assumed (section 2). Then data and context are exposed in section 3. Section 4 presents methodology used to evaluate scaling relations. Section 5 presents results, section 6 discussion and section 7 the conclusions.

2 SEISMICITY SIMILARITY PROPERTIES

2.1 Incomplete similarity and intermediate asymptotics in seismicity

Scaling can be seen as the procedure of relating values of a property from one scale to another (Hunt & Ewing, 2016). A formalization of this procedure is given by Barenblatt (2003), which starts by writing a relation between the inquired property and a number of governing parameters. In a first instance the relation can be expressed in dimensionless form using classical dimensional analysis and Pi theorem (Buckingham, 1914), thus reducing the relation's number of relevant arguments. This theorem tells that any physically significant relation (one that express a valid law to any observer, in particular those with unit measures of different magnitude) between dimensional parameters can be reduced to a relation between $p = n - k$ dimensionless parameters, with n the number of governing dimensional parameters and k the number of independent dimensions involved. Once dimension reduction is carried on then it can be determined what kind of similarity exists between the inquired property and its dimensionless arguments. If the property does not change under a change in the value of a certain dimensionless parameter, then is said that the property display complete similarity on that parameter and it can be ruled out from the formulation. On the contrary, a more general case is incomplete similarity where the dependence holds. In the fulfilling of incomplete similarity a scaling function exists having as arguments powers of dimensionless parameters. Representations arising from similarity considerations are linked to the concept of intermediate asymptotics. The property, or more general the phenomena under consideration, is analyzed at "intermediate times and distances away from boundaries such that the effects of accidental features or finer details in the spatial structure of the boundaries have disappeared but the system is still far away from its ultimately equilibrium state" (Barenblatt, 2003).

2.2 Scaling of waiting time probability distribution

In the view of seismicity as a stochastic marked point process, in which the mark in the time series corresponds to a scalar quantity and in this case to the earthquake seismic moment, the most important characteristic is waiting time τ. Here it is described using a seismic catalog data with N events obtained in a observation time τ_0, with cut-off moment M_c, localized in a seismogenic volume of characteristic linear size L_0 and produced at a mean rate $\lambda_0 = N_0/\tau_0$. Plus, it is desirable to characterize D for different exceedance moments M, and different target epicentral areas of linear dimension L. Then, D corresponds to the probability density of waiting times τ from events having moment larger or equal than M, localized in the same epicentral area of linear dimension L, from a catalog of events with moment equal or larger to M_c, localized in a seismogenic volume of linear size L_0 and produced at a rate λ_0:

$$D = f(\tau, M, L, \lambda_0, M_c, L_0), \tag{2}$$

where f is determined through data analysis. Using unit system class TML (time, moment, length), M_c, L_0 and λ_0 are selected as parameters with independent dimensions. Dimensional analysis allows us to express D in dimensionless form $\Pi = D/\lambda_0$ and to construct 3 dimensionless parameters:

$$\begin{aligned} \Pi_\tau &= \frac{\tau}{\lambda_0^{-1}} \\ \Pi_M &= \frac{M}{M_c}. \\ \Pi_L &= \frac{L}{L_0}, \end{aligned} \tag{3}$$

Then, Pi theorem allows us to express our relation in terms of a function Ψ of 3 instead of 6 parameters:

$$\Pi = \Phi\left(\Pi_\tau, \Pi_M, \Pi_L\right), \tag{4}$$

or in terms of original variables:

$$D/\lambda_0 = \Phi\left(\lambda_0\tau, M/M_c, L/L_0\right). \tag{5}$$

Now is turn to elucidate similarity of waiting time distribution with respect to these parameters. Let us introduce λ as the number of events per unit time that takes place in

an epicentral area of linear dimension L with seismic moment larger than M. Classical statistical observations account for the scaling of λ as a power of L and M (Gutenberg & Richter, 1965; Hanks & Kanamori, 1979; Kagan & Knopoff, 1980; Okubo & Aki, 1987; Aviles et al., 1987; Kossobokov & Mazhkenov, 1992): $\lambda(M, L) \propto M^{-\beta} L^{\gamma}$, then we hypothesize that the fraction of events per unit time that return after a waiting time τ in an epicentral area of linear dimension L with seismic moment larger than M also scales with powers of M and L. In our case, this corresponds to the scaling of D through its dimensionless parameters Π_M and Π_L, which can be formulated as a case of incomplete similarity:

$$\Phi = \Pi_M^{\beta} \Pi_L^{\gamma} \Psi \left(\frac{\Pi_\tau}{\Pi_M^{\beta_\tau} \Pi_L^{\gamma_\tau}} \right), \tag{6}$$

where β, γ, β_τ and γ_τ are exponents and Ψ is a function.

Additionally imposing $\beta_\tau = -\beta; \gamma_\tau = -\gamma$, this is a key assumption and implies that exponents does not depend on the waiting time, we can write:

$$D = \lambda_0 \left(\frac{M}{M_c} \right)^{\beta} \left(\frac{L}{L_0} \right)^{\gamma} \Psi \left(\lambda_0 \left(\frac{M}{M_c} \right)^{\beta} \left(\frac{L}{L_0} \right)^{\gamma} \tau \right). \tag{7}$$

Finally, replacing $\lambda = \lambda_0 \left(\frac{M}{M_c} \right)^{\beta} \left(\frac{L}{L_0} \right)^{\gamma}$ we have:

$$D = \lambda \Psi \left(\lambda \tau \right), \tag{8}$$

a expression that account for similarity of waiting time distribution on the seismic rate λ, generalized homogeneity of scaling function Ψ and incomplete similarity with seismic moment and epicentral area linear dimension. The quantity $\lambda\tau$ is called the renormalized waiting time due to being twice normalized, by the mean rate and by the powers of M and L. For the same reasons, D/λ is called the renormalized waiting time density.

The scaling function Ψ determines how the probability of observing a recurring event changes with waiting time τ elapsed from the last one, the seismic moment (or magnitude) exceedance M and the epicentral area linear dimension L, through the renormalized waiting time $\lambda\tau$. Christensen et al. (2002) analysis of California seismicity shows a regime coherent with a $\Psi \propto \tau^{-1}$ power-law scaling function in the short $\lambda\tau$-scale, later corroborated theoretically by Saichev and Sornette (2007). A transition was found around $\lambda\tau = 1$, that is, event-pairs with waiting time close to the mean waiting time in their

own L and M scale. Then a more pronounced decay of Ψ is observed for larger $\lambda\tau$-scale. This regime was first described in terms of a Poisson process for mainshocks, but later in terms of a power law (Corral, 2003).

In the next sections we will describe the Northern Chile regional setting and the data from which we will later obtain and characterize the scaling function Ψ.

3 REGIONAL SETTING AND DATA

In northern Chile, as shown in Fig. 1, there is a convergent contact, where the Nazca plate advances at $68\,\mathrm{mm\,a^{-1}}$ (Norabuena et al., 1998) in the direction N76 E (Angermann et al., 1999) with respect to the South American continent. The trace of this convergence (trench) is located roughly in a north-south direction at the greater bathymetric depths. Under the continent the subducting plate is located, which shows a simple but abrupt morphology (Contreras-Reyes et al., 2012). From 2001 onwards destructive earthquakes of different types have been recorded, with the exception of outer-rise events: at the plate interface the 2014 $Mw\,8.1$ Iquique earthquake (Ruiz et al., 2014) and the 2007 $Mw\,7.7$ Tocopilla earthquake (Delouis et al., 2009), the intermediate-depth 2005 $Mw\,7.8$ Tarapacá earthquake (Peyrat et al., 2006) and the intraplate 2001 $Mw\,6.3$ Aroma earthquake (Legrand et al., 2007).

Fig. 1 also shows the modern station network with spatial and azimuthal coverage that has allowed the construction of high-resolution seismic catalogs. We use mainly the catalog published by Sippl et al. (2018b, 2018a) which makes use of records acquired by the Chilean National Seismological Center (see Barrientos and Team (2018)) and IPOC networks, in addition to other temporary stations between the years 2007-2014. This catalog contains 101602 events relocated with the double-difference method (Waldhauser & Ellsworth, 2000), which in the study region are distributed between 0.01 and 270 km depth, with location error varying between 1.5 and 15 km depending on hypocenter location. Reported magnitudes range from 1.3 to 8.1, according to Hainzl et al. (2019) the catalog is complete for magnitudes $Ml \geq 2.7$. For comparison sake we also use USGS catalog for years 1974–2018 compiled and homogenized to moment magnitude (Mw) by Poulos et al. (2018), for this zone this catalog has 863 events with completeness magnitude of 5.0, having discarded continental plate events.

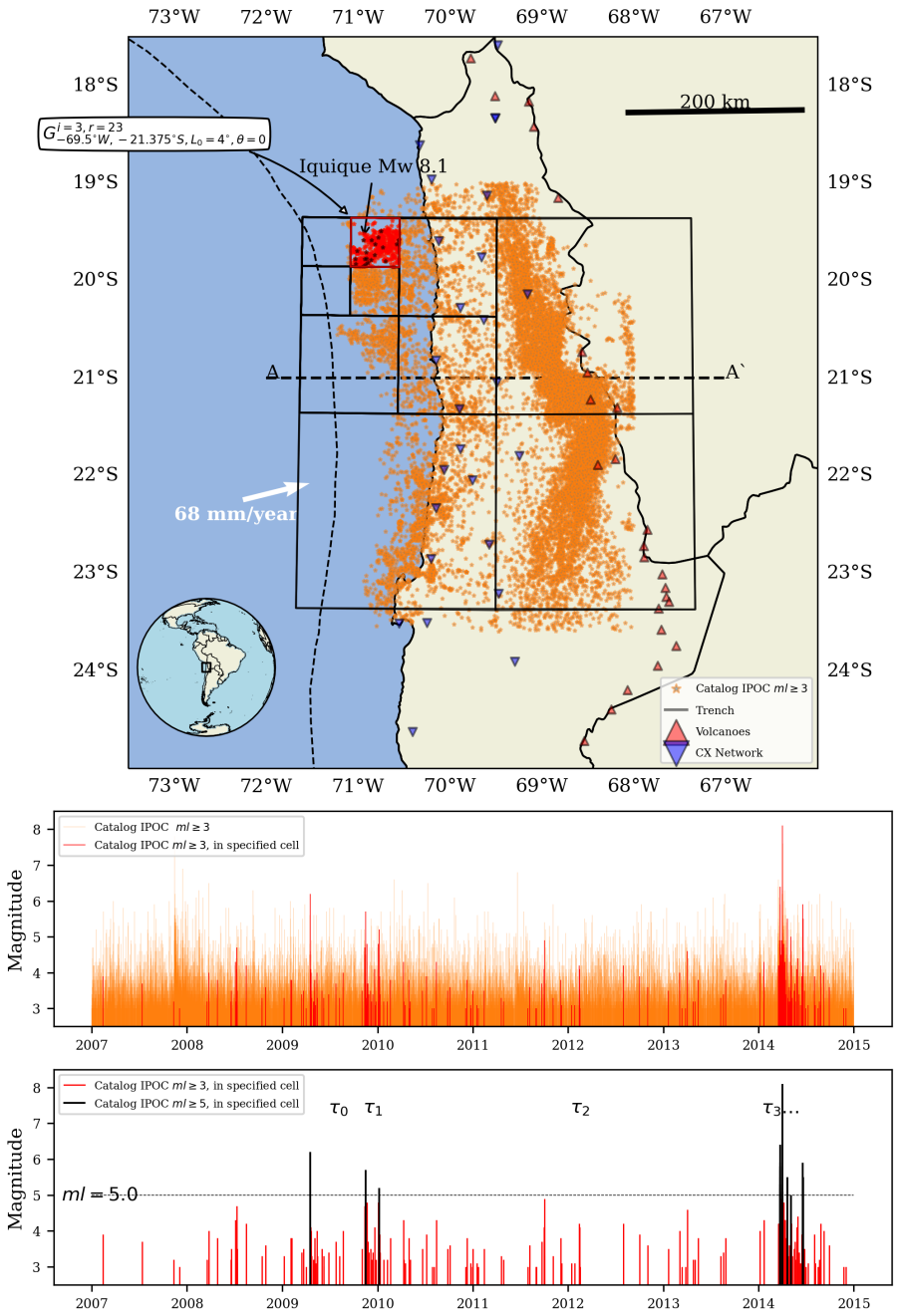

Figure 1. Top: Study zone in northern Chile between 67–73° W and 18–24° S. Permanent stations from IPOC CX Network (blue inverted triangles), active volcanoes (red triangles) and trench trace (segmented black line) are shown. White arrow shows the direction and magnitude of plate convergence vector. Epicenters from IPOC catalog with $Ml \geq 3$ are plotted (orange points). A hierarchic grid is positioned centered on 69.5° W, 21.375° E with base level linear dimension 4° (with 1° = 111 km), so that epicenters are well enough covered. A specific grid cell from hierarchy level $i = 3$ is indicated, contained epicenters are plotted in red. This subcatalog generated through selection of catalog events from a given cell is shown in time-magnitude central panel. Lower panel shows $Ml \geq 5$ magnitude slice filtering also plotted as black points in the map. From this type of subcatalogs waiting times τ can be obtained. Black arrow show $Mw\,8.1$ Iquique earthquake epicenter. A-A' cross-section is shown in Fig.2.

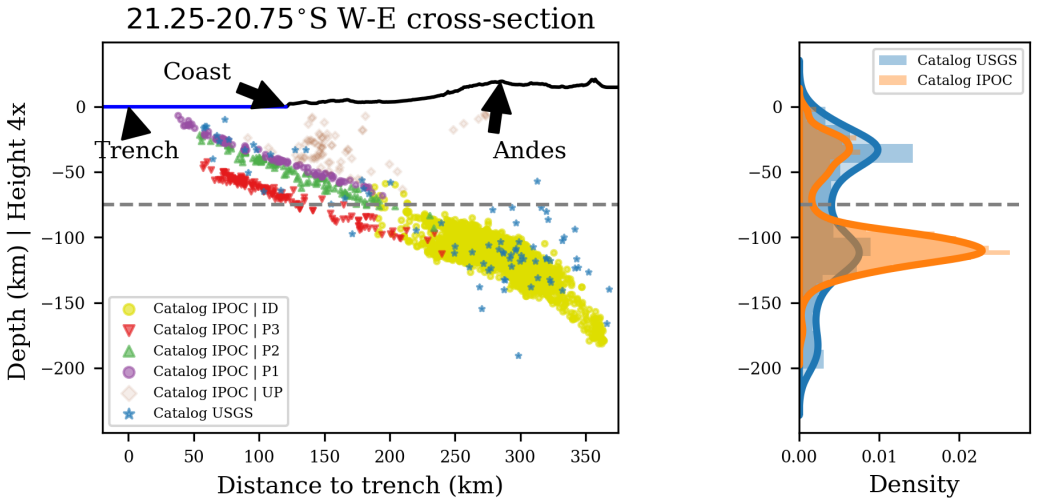

Figure 2. Left: Cross-section at 21° S between 72 and 67° W as shown in Fig. 1. Abscissa represents distance to trench in km, ordinate represents depth with respect to sea level in km. Topography is exaggerated 4 times. Features indicated are trench, coastline and Andes. Seismicity with $5.0 \leq Mw$ from USGS catalog (with continental plate events discarded) and with $3.0 \leq Ml$ for IPOC catalog is shown for events located between 21.25 and 21.75° S. In colors, according to the legend, are indicated the different seismicity clusters proposed by Sippl et al. (2018b): ID, Intermediate-Depth Cluster; P3, Lower Plane; P2, Upper Plane; P1, Plate Interface and UP, Upper Plate Cluster (not used in this study). Right: hypocenter depth density distribution for IPOC catalog and also for 1974–2018 USGS catalog, both having two distinct modes: coastal and intermediate depth seismicity, separated by a minimum at $\sim$ 75 km depth, indicated in gray discontinuous line.

Fig. 1 shows the spatial distribution of the seismic events. Two seismicity groups can be observed according to longitude: seismicity distributed around coastal zone and around the volcanic arc. Coastal seismicity is mainly associated with subduction interface between plates, notoriously denser near 20 and $23°S$ due to aftershocks following 2014 Iquique and 2007 Tocopilla earthquakes respectively. Intermediate depth seismicity corresponds to earthquakes between 80 and 270 km depth.

These two groups can be observed in the cross-section presented in Fig.2, where it can be clearly seen the distinction between coastal and intermediate depth seismicity. The former has a spatial distribution of hypocenters along a dipping plate, with clusters of seismicity separated by some vertical offset, and upper plate seismicity above this dipping plate configuration. Intermediate depth seismicity is composed by a cluster of hypocenters that fill gaps present between thin plates in coastal seismicity (Sippl et al., 2019). Both groups are separated by a minimum in the number of earthquakes around 75 km depth, as shown in the density plot on the right side of Fig.2, visible also in USGS catalog. This rough separation in coastal seismicity with depth < 75 km and intermediate depth seismicity with depth ≥ 75 km will be analyzed in subsequent sections. Justification for the occurrence of this two distinct groups can be found on literature, Oncken et al. (2003) for example showed that subducted Nazca plate reflector is no longer observed at 80–90 km due to the 650–700° isotherm that prevents stability of serpentinized oceanic crust.

To further inquire in differences between seismicity groups we will also analyze cluster distribution proposed by Sippl et al. (2018b) based on a visual inspection of hypocenter geometry, according to criteria in Table 1 of their paper. Coastal seismicity was subdivided into 3 clusters: a well-defined double seismic zone consisting of the upper P2 plane and the lower P3 plane, an observation previously noted by Comte et al. (1999); Dorbath et al. (2008); Rietbrock and Waldhauser (2004); Bloch et al. (2014) and Brudzinski et al. (2007); P1 interplate seismicity above the P2 plane associated with thrust-type earthquakes (Delouis et al., 1996). Continental seismicity is isolated and discarded for analysis in this study. Events with at depths larger than 180 km were also discarded due to poor station coverage.

4 METHODS

Empirically evaluating relationship (7) requires analyzing the temporal distribution of seismicity in the study region for different seismic moment ranges and different epicentral area linear dimension ranges. As IPOC catalog contains only local magnitudes, ratios between two seismic moments M_1 and M_2 will be of the form $M_1/M_2 = 10^{\frac{3}{2}d(Ml_1 - Ml_2)}$, where Ml_1 and Ml_2 are the respective local magnitudes and d is the slope in the moment-magnitude–local-magnitude linear regression. As in this case d is unknown, we will assume $d = 1$, which will not influence the consistency of obtained results, but could influence consistence in comparing scaling coefficients with other seismic catalogs. Then, seismic moment ranges for IPOC catalog are defined from exceedance magnitudes for $Ml = 3.0, 3.5, 4.0$ and 4.5 slices, it is important to note that the magnitude 3.0 is arbitrary, but it must be larger than the catalog cut-off magnitude. For USGS catalog in turn, seismic moment ranges for are defined from exceedance magnitudes for $Mw = 5.0$, 5.5 and 6.0 slices.

Epicentral area linear dimension ranges are defined from hierarchical grids with base level size $L_0 = 4^\circ$ which covers the whole seismogenic area, with $1^\circ = 111$ km. UTM geographic projection is used. Each grid is constructed by progressive subdivisions $L_i = L_{i-1}/4$, with $i = 1, 2, 3$ and 4, with $4, 16, 64$ and 128 cells of size $L_1 = 2^\circ$, $L_2 = 1^\circ$, $L_3 = 0.5^\circ$ and $L_4 = 0.25^\circ$ respectively. The grid used for the calculations is shown in Fig.1.

With defined M and L ranges it is possible to proceed in obtaining samples of waiting times. This is achieved through subcatalog generating process, by assigning cell coordinates to the whole catalog using a quadtree search and filtering with moment ranges defined by slices. This process is illustrated in Fig.1. Waiting times samples obtained from different cells are treated equally, this is a hypothesis of seismic homogeneity and isotropy, i.e. D waiting time probability distribution does not depend on the cell location, nor on cell orientation. In this way it is possible to say that the obtained empiric distribution comes from a cell chosen at random, which allows to collect observations from all cells in one set.

Apart from obtaining waiting time samples, mean annual number of events N_{ji} for each spatial level i and for each seismic moment j are also obtained. This allows to estimate β and γ coefficients according to the method proposed by Kossobokov and Mazhkenov (1992) (SCE, Scaling Coefficient Estimation) and suggested as a proper renormalization

factor for the waiting time distribution by Molchan (2020). Details regarding coefficients estimation procedure can be found on Nekrasova and Kossobokov (2020). It involves least-squares inversion from linear equations:

$$\log N_{ji} = (1, -\log(M_j - M_c), \log(L_i/L_0))\,(\Lambda, \beta, \gamma)^T\,, \tag{9}$$

where Λ represents the estimation of the mean seismic rate, as the logarithm of the annual number of earthquakes with seismic moment or equal than M_c in an area of linear dimension L_0. Finally, to stabilize coefficient estimation and obtain confidence intervals we repeat the sampling process by performing 100 random rotations of the grid from its center.

Once waiting times are renormalized, we provide graphical visualizations on log-log plots, note that as both axis are adimensional the axis scale is set to 1:1 in order to adequately infer qualitative characteristics, previous applications does not provide equal scaled axis which can distort the scaling function. Then, we will asses the presence or absence of the power-law asymptotic for short and long $\lambda\tau$-scale using least-squares and the likelihood method suggested by Clauset et al. (2009), respectively, as the short scale asymptotic is described qualitatively and the long scale need assessment of its heavy-tailedness, for which Clauset et al. (2009) log-likelihood ratio between power-law and exponential fit test is most adequate. Also, a graphical comparison with a exponential decay of waiting times $\Psi(\lambda\tau) = \exp(-\lambda\tau)$, which is the scaling function that model waiting times in a homogeneous Poisson Process (Langenbruch et al., 2011), will be conducted.

5 RESULTS

Table 1 shows scaling coefficients obtained through least-squares inversion of estimated renormalization factors. Λ corresponds to the logarithm of the estimated annual number of earthquakes taking place in a cell of linear dimension L_0 with seismic moment larger or equal than M_c, which essentially points to seismic activity, greater in intermediate depth clusters and interface seismicity. β corresponds to the balance between number of earthquakes generated by magnitude range, this coefficient is smaller in the case of interface seismicity than in other groups, attributable to the presence of mega-thrust earthquakes in the former. It is notable that it increases with depth from slab, this is in accordance with b-values ($\frac{3}{2}\beta$) obtained by Hainzl et al. (2019). Lastly,

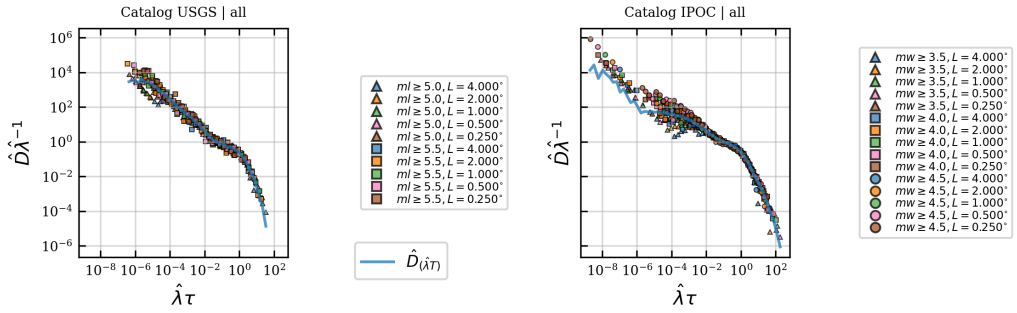

Figure 3. Renormalized empirical waiting time density $\hat{D}\hat{\lambda}^{-1}$ (ordinate) versus renormalized waiting time $\hat{\lambda}\tau$ (abscissa), for USGS (left) and IPOC (right) catalogs. Colored markers indicating different magnitude and epicentral area linear dimension ranges as shown in the legend. Blue curve corresponds to joint empirical density $\hat{D}_{(\hat{\lambda}T)}$.

γ corresponds to the correlation fractal dimension. It is the closer to 1 in the case of interface seismicity (1.1) and increases through upper (1.27) and lower (1.3) planes, with ID cluster having intermediate value 1.2. Same observation for larger fractal dimension with depth is valid for USGS catalog, although not in IPOC for this basic 75 km separation. Residuals are in the median lesser than 0.1, but considerably larger in the cases of coastal seismicity and P1.

Table 1. Scaling coefficients Λ, β, γ and least-square residuals (RES) associated to renormalization factor $\hat{\lambda}$ estimation. Values shown as the median of distribution with 95 (up) and 5 (down) percentile.

Catalog	Λ	β	γ	RES
USGS $z < 75\,\mathrm{km}$	$-6.64^{0.05}_{0.10}$	$0.59^{0.05}_{0.04}$	$1.16^{0.09}_{0.08}$	$0.04^{0.04}_{0.02}$
USGS $z \geq 75\,\mathrm{km}$	$-6.52^{0.02}_{0.08}$	$0.82^{0.03}_{0.07}$	$1.32^{0.04}_{0.10}$	$0.06^{0.11}_{0.02}$
USGS all	$-6.38^{0.03}_{0.05}$	$0.65^{0.04}_{0.04}$	$1.45^{0.06}_{0.07}$	$0.09^{0.05}_{0.03}$
IPOC $z < 75\,\mathrm{km}$	$-4.81^{0.06}_{0.08}$	$0.45^{0.01}_{0.01}$	$1.23^{0.05}_{0.06}$	$0.06^{0.04}_{0.03}$
IPOC $z \geq 75\,\mathrm{km}$	$-4.17^{0.02}_{0.04}$	$0.64^{0.01}_{0.01}$	$1.22^{0.02}_{0.02}$	$0.04^{0.02}_{0.01}$
IPOC all	$-4.11^{0.01}_{0.01}$	$0.61^{0.01}_{0.02}$	$1.40^{0.04}_{0.04}$	$0.06^{0.03}_{0.03}$
IPOC P1	$-4.98^{0.05}_{0.11}$	$0.43^{0.02}_{0.02}$	$1.11^{0.06}_{0.07}$	$0.07^{0.07}_{0.04}$
IPOC P2	$-5.31^{0.02}_{0.04}$	$0.50^{0.02}_{0.02}$	$1.27^{0.06}_{0.10}$	$0.05^{0.04}_{0.02}$
IPOC P3	$-5.70^{0.01}_{0.04}$	$0.52^{0.05}_{0.03}$	$1.30^{0.02}_{0.04}$	$0.03^{0.02}_{0.02}$
IPOC ID	$-4.18^{0.02}_{0.05}$	$0.64^{0.01}_{0.01}$	$1.20^{0.02}_{0.02}$	$0.04^{0.03}_{0.01}$

Fig. 3 shows the renormalized waiting time distribution as a function of the renormalized waiting times for the two catalogs (circumflex diacritic on quantities denotes empirical estimates). An overall collapse of the distributions resulting from the renormal-

ization process is observed. It can be noted that for $\hat{\lambda}\tau < 10^{-2}$ divergence of curves is observed, not collapsing all in one function, most notably in IPOC catalog. This can be due to the undersampling of very short waiting times and/or due to the mixing of distributions from different scaling and functions and/or coefficients. This latter factor was noted by Davidsen and Goltz (2004), they found that different values of fractal dimensions where able to fit different regions of waiting time distribution in Southern California and Island catalogs. Above the curves we have plotted the joint density function of all sampled renormalized waiting times (rather than separated in their respective M and L ranges), which is marked by the curve (blue) corresponding to the distribution obtained by considering all interevent times (indicated as $\hat{D}_{\hat{\lambda}T}$). This curve represents the overall behaviour of scaling function Ψ, although it can be noted that for $\hat{\lambda}\tau < 10^{-2}$ it tends to go below individual distributions, mostly

Scaling function Ψ is generally decreasing for all clusters. It can be noted that the ordinate value $\hat{D}\hat{\lambda}^{-1} = 1$ marks the transition from a gentler to a stepper descent, with a middle slope in between that ends in the abscissa $\hat{\lambda}\tau = 1$. This means points located to the left of the transition corresponds to types of recurrences happening with frequency lesser than expected from the mean rate: $\hat{D} < \hat{\lambda}$ and vice versa. Moreover, renormalized waiting times with $\hat{\lambda}\tau < 1$ means waiting times shorter than the mean waiting time $\hat{\lambda}^{-1}$ and vice versa. Then, transition region is composed by recurrences with waiting times shorter than the mean waiting time that occur with frequency larger than the expected from the mean frequency. This transition region will be important when comparing waiting time distributions for different groups and cluster, as shown next.

Fig. 4 allows us to compare scaling functions Ψ for the USGS and IPOC catalogs in the coastal ($z < 75$ km) and intermediate seismicity groups ($z \geq 75$ km). Furthermore, analysis for clusters P1, P2, P3 and ID are also shown. Figures are organized such as easily visualize the differences. Left column with coastal seismicity and clusters P1 and P2 posses a steep power law descent in the region before the transition, with coefficients $\alpha \sim 0.7$ in the case of P2 and near 0.9–1 in other cases, comparable to Omori coefficient for aftershocks. Right column in turn, with intermediate depth seismicity, P3 and ID clusters shows gentler slope power law segments with $0.2 < \alpha < 0.6$. The other remarkable difference between columns is the form and values of Ψ scaling function in the transition region. For comparing, a exponential function is shown in each figure. In left columns coastal seismicity, P1 and P2 clusters scaling functions do not agree with

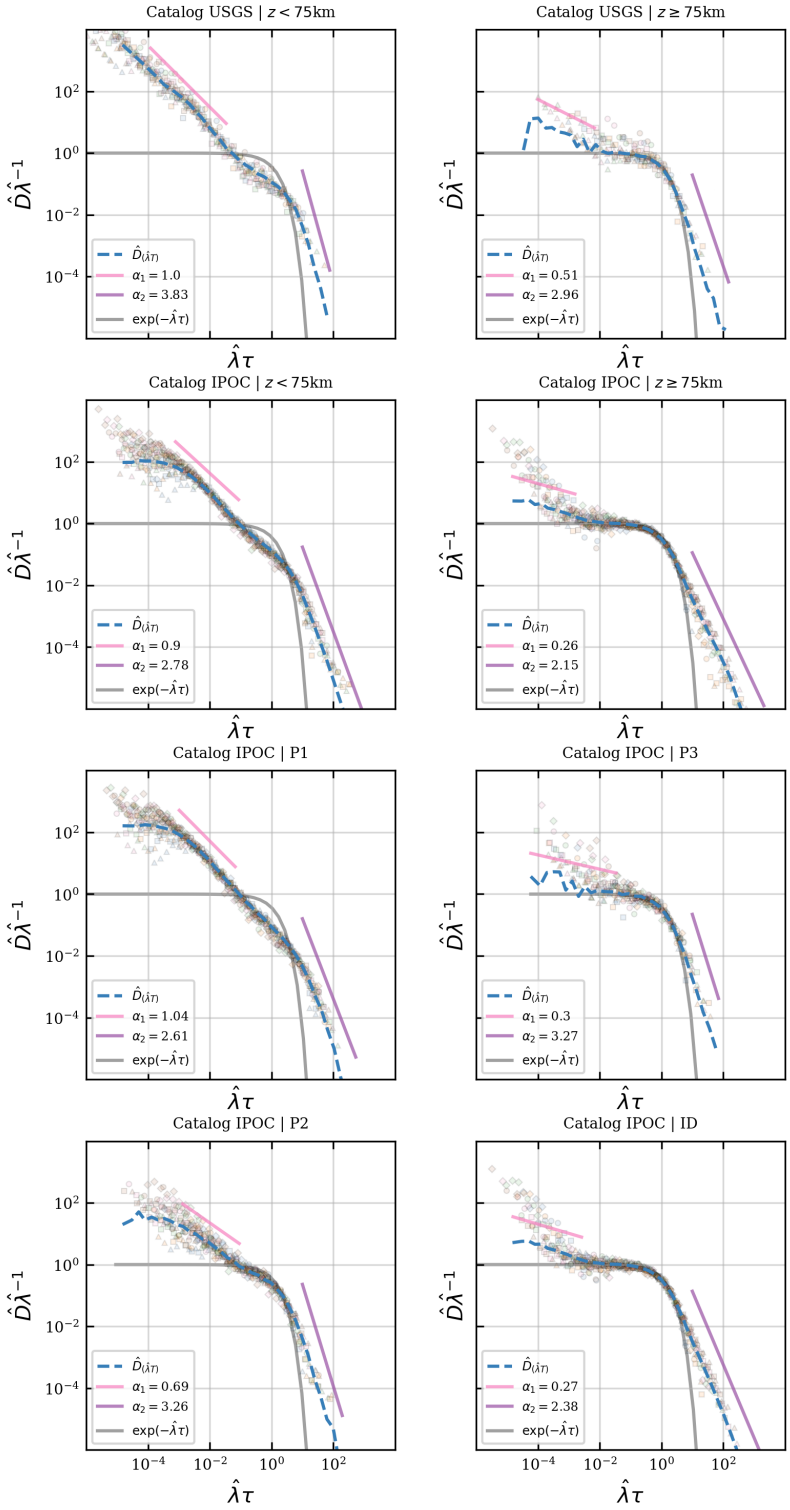

Figure 4. Renormalized empirical waiting time density $\hat{D}\hat{\lambda}^{-1}$ (ordinate) versus renormalized waiting time $\hat{\lambda}\tau$ (abscissa) for USGS and IPOC coastal P1 and P2 clusters (left) and USGS and IPOC intermediate depth P3 and ID clusters (right). Dashed blue curve corresponds to joint empirical density $\hat{D}_{(\hat{\lambda}T)}$. Solid lines corresponds to fitted power law segments and exponential scaling function. Markers are the same as for previous figures, representing individual scale distribution.

a exponential decay in the transition region. In fact, $\Psi < \exp^{-\hat{\lambda}\tau}$, meaning that observed recurrence density is less abundant than the expected for a pure Poisson Process. In turn, in the right column intermediate depth seismicity, ID and P3 clusters have scaling function Ψ that agree well with a exponential function in the transition region.

Finally, after the transition region all scaling functions seem to posses a power law decay. We tested this assumption with likelihood ratio between power law and exponential fits (Clauset et al., 2009), obtaining positive values in all cases, but significance only for IPOC catalog except P3, see Table 2 in Appendix A, which could be attributed to scarcity of data in this cluster and in USGS catalog.

6 DISCUSSION

Fig. 5 synthesizes our characterization of waiting time distribution. It is possible to observe 3 regions, labelled as A, B and C. Region A corresponds to clustered seismicity and consists of recurrences with $\hat{D} > \lambda$, which means an surplus of probability with respect to an exponential function. The fitted power-law scaling exponent modulate the degree of productivity of clustered seismicity, higher for interface seismicity and lower for non-interface seismicity, with upper plane seismicity in between, with limiting value $\alpha_1 = 1$, as in Omori Law and deduced from analytic formulation by Saichev and Sornette (2007).

Region B corresponds to recurrences near the mean waiting time $\tau = \hat{\lambda}^{-1}$, in which a deficit of waiting time probability with respect to exponential function exists for interface seismicity and upper plane, while non-interface seismicity agree with the exponential function. This latter observation was also made for intermediate depth seismicity in Vrancea region (Enescu et al., 2008). . Observations also agree well with those of Telesca et al. (2020) performed in the same catalog, they found interplate clustering persists even after declustering the catalog, thus correlations dominate, while lower plane seismicity maintains its poisonnean nature. Interestingly enough, our results does not agree with tests of exponential decay performed by authors of compiled USGS catalog (Poulos et al., 2018). It must be noted that our results are scale independent, as we incorporated several moment and epicentral area linear dimension ranges.

Region C corresponds to recurrences of waiting times much larger than the mean waiting time, in this region all divisions have power-law decay of their scaling functions,

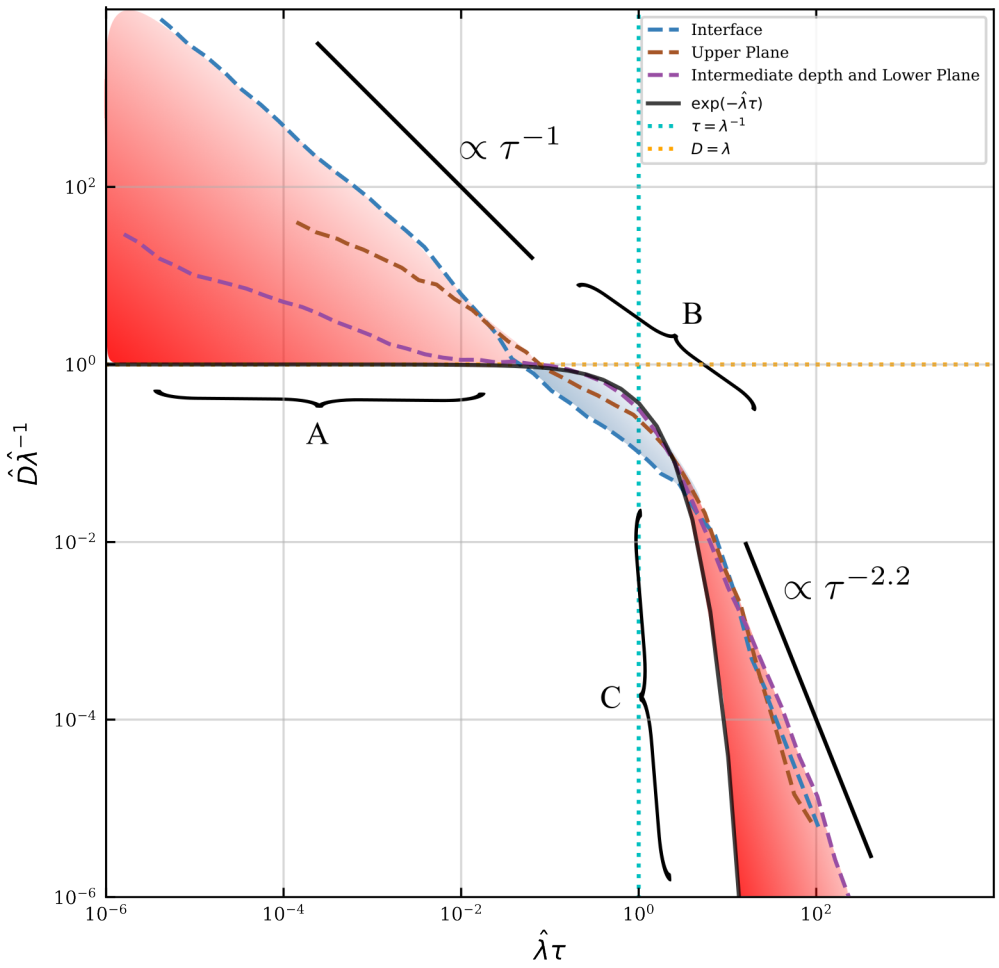

Figure 5. A: surplus of probability with respect to exponential function due to short-scale clustering - all divisions (with differences in productivity). B: deficit of probability with respect to exponential function in interface seismicity and exponentially distributed waiting times for intermediate depth and lower plane. C: surplus of probability with respect to exponential function - all divisions.

which mean a surplus of probability with respect to exponential function. The power law exponent there seems to depend on each division number of events and with cutoff magnitude, with the coefficient 2.2 as a limiting case, this one was stated as universal in Corral (2004). Power-law behaviour is related to long-term clustering, first described by (Kagan & Jackson, 1991). Recent papers on global scale and long-term agree with departure from exponential decay (Griffin et al., 2020; Chen et al., 2020)

What are the consequences for seismic hazard? If for a specified moment-area scale (this is, specifying a target linear dimension and a target magnitude exceedance) an earthquake has been expected for a time short enough (according to scale) then it is expected with high probability that another one occurs close in time, specially for coastal seismicity, and more particularly for interface seismicity, once it's hypocenter is finely calculated and established that it occurred there. It can be noted that as no distinction is made between foreshocks, aftershocks and mainshocks, every other earthquake taking place restarts the waiting time count. Then, if an earthquake has been waited sufficiently enough to enter region B, it is to be expected that it occurs with a probability that is inferior or alike to what an exponential function model, in the cases of interface seismicity and non-interface seismicity, respectively.

After the transition, in region C, probability is power-law distributed, at least in IPOC catalog except lower plane, a fact that does not disappear by declustering the catalog, meaning that there is a larger density of recurrences than expected from exponential decay, thus exponential assumption underestimates hazard. Although the statistical test to verify power-law does not yield positive results in medium-term USGS catalog, it is clear from results that scaling functions posses a decay that is slower than a exponential, this could be modelled with Gamma or Weibull distributions, as previous literature suggests.

The key factor that differentiates interface seismicity and upper plane from intermediate depth seismicity and lower plane seismicity is that the former occurs in a context of interacting plates. This interaction is what then produces correlations between events, noted as sharp power law decay in the short scale and departure from exponential function in the central transition regime. Hainzl et al. (2019) noted that aftershock productivity decreases with decreasing distance from trench along slab and associated it to decreasing interplate coupling, meanwhile Cabrera et al. (2021) note decreasing af-

tershock productivity with distance from slab and associated it with local isotherm. Both observations agree with our results and highlight the importance of plate interaction in the seismicity generation process. What is also remarkable is that the lower plane seismicity and intermediate depth have similar behaviour in spite of being located in different tectonic contexts, suggesting that they have a common generating mechanism.

Is there any relation between space-moment scaling coefficients β and γ and the described waiting time distributions? Our results indicate that interface seismicity have lower β hence b-value and fractal dimension than non-interface seismicity. This could be due to interface seismicity dominated by patches of asperities, i.e. regions of correlated state of stress. Higher values of fractal dimension means epicenters filling a plane, while values closer to 1 means epicenters concentrated along linear features. In the case of interface seismicity, presence of asperities could concentrate epicenters along their borders, thus lowering fractal dimension, and as asperities have potential to generate earthquakes of large magnitude this lowers also the b-value. Besides, residual stresses in asperities could produce higher number of clustered seismicity and aftershocks. In turn, non-interface seismicity is clearly dispersed and more homogeneously distributed, suggesting a more random distribution of stresses hence raising fractal dimension, raising b-value and lowering short-scale clustering. We here need to call for caution since distributions for scaling coefficients from random sampling are skewed and sometimes bimodal, this could be due to latitudinal variations and more detailed studies and exploration in other subduction regions are needed in order to establish the significance of differences found.

Other aspect that needs to be remarked is the existence of similarity breaking in the short scale, previously reported by Davidsen and Goltz (2004). This must be due to the presence of different scaling coefficients, in particular fractal dimensions. In that case is not data incompleteness but a dynamic property of the system the one that is showing.

Due to results obtained in this study, we speculate that continental, outer rise and deep focus earthquakes also posses distinct waiting time scaling behaviour, that future studies need to analyze. Furthermore, interactions between interface and other contexts is starting to be quantified (e.g. with intermediate depth (Jara et al., 2017; Aden-Antóniow et al., 2020), with continental seismicity (Pastén-Araya et al., 2021)). Separation between different contexts can improve, a useful resource could be the use of focal mechanism in-

versions using near source records (Derode et al., 2019), already operative in the region. Our scaling analysis although minimalist as contains only governing parameters obtainable from seismic catalogs, have the potential to incorporate more variables that could in the future help to elucidate the origin of differences found in this study, detect interactions and allow the integration of seismicity catalogs with other kinds of data.

7 CONCLUSIONS

In this study we have used an approach based on a unified scaling law for seismicity, that we derived from similarity principles, to characterize seismic catalogues available for the Northern Chile subduction zone. Although the scaling approach only incorporate variables available in seismic catalogues, it is enough to provide evidence of distinct behaviours for different spatial domains. A rough division distinguishes coastal from intermediate depth seismicity, the former with marked spatio-temporal clustering behaviour and the latter with events more broadly spread in space and time. The availability of the IPOC catalog with large spatial resolution and small magnitude completeness allowed us to discern distinct behaviours inside the coastal seismicity, with lower plane activity that resembles intermediate depth seismicity, and with an upper plate activity with an intermediate behaviour. As stated in the introduction, earthquakes from these different types have different potential hazard due to different source characteristics and grounds acceleration. The classification of earthquakes according to spatio temporal-moment organization generates additional complexity to seismic hazard estimation, which requires additional efforts to enhance instrumental monitoring and hypocentre location analysis.

ACKNOWLEDGMENTS

CS: Conceptualization, Methodology, Software, Formal Analysis, Investigation, Writing - Original Draft, Data Curation, Visualization. PT: Conceptualization, Methodology, Validation, Formal Analysis, Writing- Original draft. RM: Formal Analysis, Resources, Validation, Writing - Review and Editing. JC: Resources, Supervision, Project administration, Funding Adquisition, Writing - Review and Editing.

CS and JC acknowledge financial support from Fondecyt Project 1170218. RM acknowledge financial support from Fondecyt Project 1211105. CS, PT and RM acknowl-

edge financial support from the Seismic Risk Program (PRS) of University of Chile. We thanks IPOC collaboration affiliated institutions (German Research Center For Geosciences (GFZ), Germany; GEOSCOPE Program of Institut de Physique du Globe de Paris and C.N.R.S., France; Centro Sismológico Nacional (CSN) of Faculty of Physical and Mathematical Sciences of University of Chile; and Universidad Católica del Norte, Chile) and GFZ German Research Centre For Geosciences and Institut Des Sciences De L'Univers-Centre National De La Recherche CNRS-INSU (2006); Wigger et al. (2012); Asch et al. (2011); Cesca et al. (2018); Barrientos and Team (2018); GFZ (1993) for the seismic network maintenance that made this work possible.

DATA AVAILABILITY

The processed data and code used for making tables and figures in this study are available at Repositorio de Datos de Investigación de la Universidad de Chile via https://doi.org/10.34691/FK2/GGHMFZ.

References

Aden-Antóniow, F., Satriano, C., Bernard, P., Poiata, N., Aissaoui, E.-M., Vilotte, J.-P., & Frank, W. B. (2020). Statistical analysis of the preparatory phase of the mw 8.1 iquique earthquake, chile. *Journal of Geophysical Research: Solid Earth*, *125*(6), e2019JB019337. Retrieved from `https://agupubs.onlinelibrary.wiley.com/doi/abs/10.1029/2019JB019337` (e2019JB019337 10.1029/2019JB019337) doi: https://doi.org/10.1029/2019JB019337

Angermann, D., Klotz, J., & Reigber, C. (1999). Space-geodetic estimation of the nazca-south america euler vector. *Earth and Planetary Science Letters*, *171*(3), 329–334.

Asch, G., Tilmann, F., Schurr, B., & Ryberg, T. (2011). *Seismic network 5e: Minas project (2011/2013).* Retrieved from `https://doi:10.14470/ab466166`

Astroza, M., Sandoval, M., & Kausel, E. (2005). Estudio comparativo de los efectos de los sismos chilenos de subducción del tipo intraplaca de profundidad intermedia. *IX Jornadas de Sismología e Ingeniería Antisísmica, Concepción, Chile*.

Aviles, C. A., Scholz, C. H., & Boatwright, J. (1987). Fractal analysis applied

to characteristic segments of the san andreas fault. *Journal of Geophysical Research: Solid Earth*, *92*(B1), 331-344. Retrieved from https://agupubs.onlinelibrary.wiley.com/doi/abs/10.1029/JB092iB01p00331 doi: https://doi.org/10.1029/JB092iB01p00331

Baiesi, M., & Paczuski, M. (2004). Scale-free networks of earthquakes and aftershocks. *Physical review E*, *69*(6), 066106.

Barenblatt, G. I. (2003). Dimensional analysis and physical similarity. In *Scaling* (p. 12–51). Cambridge University Press. doi: 10.1017/CBO9780511814921.004

Barrientos, S., & Team, N. S. C. C. (2018). The seismic network of chile. *Seismological Research Letters*, *89*(2A), 467–474.

Bloch, W., Kummerow, J., Salazar, P., Wigger, P., & Shapiro, S. (2014). High-resolution image of the north chilean subduction zone: seismicity, reflectivity and fluids. *Geophysical Journal International*, *197*(3), 1744–1749.

Brudzinski, M. R., Thurber, C. H., Hacker, B. R., & Engdahl, E. R. (2007). Global prevalence of double benioff zones. *Science*, *316*(5830), 1472–1474.

Buckingham, E. (1914). On physically similar systems; illustrations oa the use of dimensional equations. *Physical review*, *4*(4), 345.

Cabrera, L., Ruiz, S., Poli, P., Contreras-Reyes, E., Osses, A., & Mancini, R. (2021). Northern chile intermediate-depth earthquakes controlled by plate hydration. *Geophysical Journal International*, *226*(1), 78–90.

Cesca, S., Sobiesiak, M., Tassara, C., Olcay, M., Günther, E., Mikulla, S., & Dahm, T. (2018). *The iquique local network and picarray* (Tech. Rep.). Potsdam, Germany: GFZ German Research Centre for Geosciences.

Chen, Y., Liu, M., & Luo, G. (2020, 04). Complex Temporal Patterns of Large Earthquakes: Devil's Staircases. *Bulletin of the Seismological Society of America*, *110*(3), 1064-1076. Retrieved from https://doi.org/10.1785/0120190148 doi: 10.1785/0120190148

Christensen, K., Danon, L., Scanlon, T., & Bak, P. (2002). Unified scaling law for earthquakes. *Proceedings of the National Academy of Sciences*, *99*(suppl 1), 2509–2513. Retrieved from https://www.pnas.org/content/99/suppl_1/2509 doi: 10.1073/pnas.012581099

Clauset, A., Shalizi, C. R., & Newman, M. E. (2009). Power-law distributions in em-

pirical data. *SIAM review*, *51*(4), 661–703.

Comte, D., Dorbath, L., Pardo, M., Monfret, T., Haessler, H., Rivera, L., ... Meneses, C. (1999). A double-layered seismic zone in arica, northern chile. *Geophysical Research Letters*, *26*(13), 1965–1968.

Contreras-Reyes, E., Jara, J., Grevemeyer, I., Ruiz, S., & Carrizo, D. (2012). Abrupt change in the dip of the subducting plate beneath north chile. *Nature Geoscience*, *5*(5), 342.

Corral, Á. (2003). Local distributions and rate fluctuations in a unified scaling law for earthquakes. *Physical Review E*, *68*, 035102.

Corral, Á. (2004). Universal local versus unified global scaling laws in the statistics of seismicity. *Physica A: Statistical Mechanics and its Applications*, *340*(4), 590–597.

Davidsen, J., & Goltz, C. (2004). Are seismic waiting time distributions universal? *Geophysical research letters*, *31*(21).

Delouis, B., Cisternas, A., Dorbath, L., Rivera, L., & Kausel, E. (1996). The andean subduction zone between 22 and 25 s (northern chile): Precise geometry and state of stress. *Tectonophysics*, *259*(1-3), 81–100.

Delouis, B., Pardo, M., Legrand, D., & Monfret, T. (2009). The m w 7.7 tocopilla earthquake of 14 november 2007 at the southern edge of the northern chile seismic gap: rupture in the deep part of the coupled plate interface. *Bulletin of the Seismological Society of America*, *99*(1), 87–94.

Derode, B., & Campos, J. (2019). Energy budget of intermediate-depth earthquakes in northern chile: comparison with shallow earthquakes and implications of rupture velocity models used. *Geophysical Research Letters*, *46*(5), 2484–2493.

Derode, B., Delouis, B., & Campos, J. (2019). Systematic determination of focal mechanisms over a wide magnitude range: Insights from the real-time fmnear implementation in chile from 2015 to 2017. *Seismological Research Letters*, *90*(3), 1285–1295.

Dorbath, C., Gerbault, M., Carlier, G., & Guiraud, M. (2008). Double seismic zone of the nazca plate in northern chile: High-resolution velocity structure, petrological implications, and thermomechanical modeling. *Geochemistry, Geophysics, Geosystems*, *9*(7).

Enescu, B., Struzik, Z., & Kiyono, K. (2008). On the recurrence time of earth-

quakes: insight from vrancea (romania) intermediate-depth events. *Geophysical Journal International*, *172*(1), 395–404.

GFZ, D. G. (1993). *Geofon seismic network* (Tech. Rep.). Retrieved from https://doi:10.14470/TR560404

GFZ German Research Centre For Geosciences, & Institut Des Sciences De L'Univers-Centre National De La Recherche CNRS-INSU. (2006). *Ipoc seismic network.* Integrated Plate boundary Observatory Chile - IPOC. Retrieved from http://geofon.gfz-potsdam.de/doi/network/CX doi: 10.14470/PK615318

Griffin, J. D., Stirling, M. W., & Wang, T. (2020). Periodicity and clustering in the long-term earthquake record. *Geophysical Research Letters*, *47*(22), e2020GL089272. Retrieved from https://agupubs.onlinelibrary.wiley.com/doi/abs/10.1029/2020GL089272 (e2020GL089272 2020GL089272) doi: https://doi.org/10.1029/2020GL089272

Gutenberg, B., & Richter, C. (1965). *Seismicity of the earth and associated phenomena*. Hafner Publishing Company. Retrieved from https://books.google.cl/books?id=qprAuQEACAAJ

Hainzl, S., Sippl, C., & Schurr, B. (2019). Linear relationship between aftershock productivity and seismic coupling in the northern chile subduction zone. *Journal of Geophysical Research: Solid Earth*, *124*, 8726–8738.

Hanks, T. C., & Kanamori, H. (1979). A moment magnitude scale. *Journal of Geophysical Research: Solid Earth*, *84*(B5), 2348-2350. Retrieved from https://agupubs.onlinelibrary.wiley.com/doi/abs/10.1029/JB084iB05p02348 doi: https://doi.org/10.1029/JB084iB05p02348

Hunt, A., & Ewing, R. P. (2016). Scaling. In *The handbook of groundwater engineering* (pp. 477–514). CRC Press.

Jara, J., Socquet, A., Marsan, D., & Bouchon, M. (2017). Long-term interactions between intermediate depth and shallow seismicity in north chile subduction zone. *Geophysical Research Letters*, *44*(18), 9283–9292.

Kagan, Y. Y., & Jackson, D. D. (1991). Long-term earthquake clustering. *Geophysical Journal International*, *104*(1), 117–133.

Kagan, Y. Y., & Knopoff, L. (1980). Spatial distribution of earthquakes: the two-point correlation function. *Geophysical Journal of the Royal Astronomical Society*, *62*(2), 303-320. Retrieved from https://onlinelibrary.wiley.com/

doi/abs/10.1111/j.1365-246X.1980.tb04857.x doi: 10.1111/j.1365-246X.1980.tb04857.x

Kausel, E., & Campos, J. (1992). The ms= 8 tensional earthquake of 9 december 1950 of northern chile and its relation to the seismic potential of the region. *Physics of the earth and planetary interiors*, *72*(3-4), 220–235.

Kossobokov, V. G., & Mazhkenov, S. A. (1992). On similarity in the spatial distribution of seismicity. In *Selected papers from volumes 22 and 23 of vychislitel'naya seysmologiya* (p. 6-15). American Geophysical Union (AGU). Retrieved from https://agupubs.onlinelibrary.wiley.com/doi/abs/10.1029/CS001p0006 doi: https://doi.org/10.1029/CS001p0006

Langenbruch, C., Dinske, C., & Shapiro, S. (2011). Inter event times of fluid induced earthquakes suggest their poisson nature. *Geophysical Research Letters*, *38*(21).

Legrand, D., Delouis, B., Dorbath, L., David, C., Campos, J., Marquez, L., ... Comte, D. (2007). Source parameters of the mw= 6.3 aroma crustal earthquake of july 24, 2001 (northern chile), and its aftershock sequence. *Journal of south American earth sciences*, *24*(1), 58–68.

Leyton, F., Ruiz, J., Campos, J., & Kausel, E. (2009). Intraplate and interplate earthquakes in chilean subduction zone: A theoretical and observational comparison. *Physics of the Earth and Planetary interiors*, *175*(1-2), 37–46.

Molchan, G. (2020). Fractal seismicity and seismic risk. *Izvestiya, Physics of the Solid Earth*, *56*(1), 66–73.

Nekrasova, A., & Kossobokov, V. (2020). The unified scaling law for earthquakes. *Journal of Volcanology and Seismology*, *14*(6), 353–372.

Norabuena, E., Leffler-Griffin, L., Mao, A., Dixon, T., Stein, S., Sacks, I. S., ... Ellis, M. (1998). Space geodetic observations of nazca-south america convergence across the central andes. *Science*, *279*(5349), 358–362. Retrieved from https://science.sciencemag.org/content/279/5349/358 doi: 10.1126/science.279.5349.358

Okubo, P. G., & Aki, K. (1987). Fractal geometry in the san andreas fault system. *Journal of Geophysical Research: Solid Earth*, *92*(B1), 345-355. Retrieved from https://agupubs.onlinelibrary.wiley.com/doi/abs/10.1029/JB092iB01p00345 doi: https://doi.org/10.1029/JB092iB01p00345

Oncken, O., Asch, G., Haberland, C., Metchie, J., Sobolev, S., Stiller, M., ... Rietbrock, A. (2003). Seismic imaging of a convergent continental margin and plateau in the central andes (andean continental research project 1996 (ancorp'96)). *Journal of Geophysical Research: Solid Earth*, *108*(B7). Retrieved from https://agupubs.onlinelibrary.wiley.com/doi/abs/10.1029/2002JB001771 doi: https://doi.org/10.1029/2002JB001771

Otarola, C., Ruiz, S., Herrera, C., Madariaga, R., & Siegel, C. (2021). Dynamic rupture of subduction earthquakes located near the trench. *Earth and Planetary Science Letters*, *562*, 116842.

Pastén-Araya, F., Potin, B., Ruiz, S., Zerbst, L., Aden-Antoniów, F., Azúa, K., ... Fuenzalida, A. (2021). Seismicity in the upper plate of the northern chilean offshore forearc: Evidence of splay fault south of the mejillones peninsula. *Tectonophysics*, *800*, 228706. Retrieved from https://www.sciencedirect.com/science/article/pii/S0040195120303899 doi: https://doi.org/10.1016/j.tecto.2020.228706

Peyrat, S., Campos, J., de Chabalier, J. B., Perez, A., Bonvalot, S., Bouin, M.-P., ... Vilotte, J.-P. (2006). Tarapacá intermediate-depth earthquake (mw 7.7, 2005, northern chile): A slab-pull event with horizontal fault plane constrained from seismologic and geodetic observations. *Geophysical Research Letters*, *33*(22). Retrieved from https://agupubs.onlinelibrary.wiley.com/doi/abs/10.1029/2006GL027710 doi: https://doi.org/10.1029/2006GL027710

Poulos, A., Monsalve, M., Zamora, N., & de la Llera, J. C. (2018). An updated recurrence model for chilean subduction seismicity and statistical validation of its poisson nature. *Bulletin of the Seismological Society of America*, *109*(1), 66–74.

Rietbrock, A., & Waldhauser, F. (2004). A narrowly spaced double-seismic zone in the subducting nazca plate. *Geophysical Research Letters*, *31*(10).

Ruiz, S., Metois, M., Fuenzalida, A., Ruiz, J., Leyton, F., Grandin, R., ... Campos, J. (2014). Intense foreshocks and a slow slip event preceded the 2014 iquique mw 8.1 earthquake. *Science*, *345*(6201), 1165–1169.

Saichev, A., & Sornette, D. (2007). Theory of earthquake recurrence times. *Journal of Geophysical Research: Solid Earth*, *112*(B4).

Sippl, C., Schurr, B., Asch, G., & Kummerow, J. (2018a). *Catalogue of earthquake*

hypocenters for northern chile compiled from ipoc (plus auxiliary) seismic stations. GFZ Data Services. Retrieved from http://doi.org/10.5880/GFZ.4.1.2018.001

Sippl, C., Schurr, B., Asch, G., & Kummerow, J. (2018b). Seismicity structure of the northern chile forearc from¿ 100,000 double-difference relocated hypocenters. *Journal of Geophysical Research: Solid Earth*, *123*(5), 4063–4087.

Sippl, C., Schurr, B., John, T., & Hainzl, S. (2019). Filling the gap in a double seismic zone: Intraslab seismicity in northern chile. *Lithos*, *346*, 105155.

Telesca, L., Pastén, D., & Muñoz, V. (2020). Analysis of time dynamical features in intraplate versus interplate seismicity: The case study of iquique area (chile). *Pure and Applied Geophysics*, *177*(10), 4755–4773.

Waldhauser, F., & Ellsworth, W. L. (2000). A double-difference earthquake location algorithm: Method and application to the northern hayward fault, california. *Bulletin of the seismological society of America*, *90*(6), 1353–1368.

Wigger, P., Salazar, P., Kummerow, J., Bloch, W., Asch, G., & Shapiro, S. W. (2012). *Fissure- and atacama-fault seismic network (2005/2012).* Retrieved from https://doi.org/10.14470/3S7550699980

Zaliapin, I., Gabrielov, A., Keilis-Borok, V., & Wong, H. (2008). Clustering analysis of seismicity and aftershock identification. *Physical review letters*, *101*(1), 018501.

Appendix A

Table 2. Power-law coefficients for short (α_1) and long (α_2) scale decay of scaling function, with respective standard deviations (σ_1 and σ_2). Values shown as the median of distribution with 95 (up) and 5 (down) percentile. Likelihood ratio power law test results *PL test* and associated p significance value are shown.

Catalog	α_1	σ_1	α_2	σ_2	p	PL test
USGS $z < 75$km — Full	$-1.01^{0.05}_{0.03}$	$0.03^{0.01}_{0.01}$	$3.82^{0.56}_{0.87}$	$0.48^{0.19}_{0.16}$	0.47	False
USGS $z \geq 75$km — Full	$-0.52^{0.17}_{0.21}$	$0.11^{0.09}_{0.05}$	$3.04^{0.56}_{0.49}$	$0.54^{0.18}_{0.15}$	0.30	False
USGS all — Full	$-0.91^{0.06}_{0.04}$	$0.03^{0.01}_{0.01}$	$3.78^{0.57}_{0.56}$	$0.48^{0.11}_{0.10}$	0.51	False
IPOC $z < 75$km — Full	$-0.89^{0.02}_{0.03}$	$0.04^{0.00}_{0.00}$	$2.75^{0.19}_{0.24}$	$0.05^{0.01}_{0.01}$	0.00	True
IPOC $z \geq 75$km — Full	$-0.26^{0.04}_{0.06}$	$0.04^{0.02}_{0.01}$	$2.15^{0.09}_{0.15}$	$0.02^{0.00}_{0.00}$	0.00	True
IPOC all — Full	$-0.51^{0.04}_{0.03}$	$0.01^{0.00}_{0.00}$	$2.47^{0.09}_{0.06}$	$0.02^{0.00}_{0.00}$	0.00	True
IPOC P1 — Full	$-1.03^{0.03}_{0.02}$	$0.03^{0.01}_{0.00}$	$2.63^{0.09}_{0.16}$	$0.06^{0.01}_{0.01}$	0.03	True
IPOC P2 — Full	$-0.69^{0.03}_{0.03}$	$0.02^{0.01}_{0.01}$	$3.26^{0.38}_{0.24}$	$0.17^{0.02}_{0.03}$	0.01	True
IPOC P3 — Full	$-0.29^{0.17}_{0.14}$	$0.08^{0.05}_{0.03}$	$3.28^{0.33}_{0.42}$	$0.41^{0.07}_{0.11}$	0.29	False
IPOC ID — Full	$-0.26^{0.03}_{0.06}$	$0.02^{0.01}_{0.01}$	$2.37^{0.13}_{0.18}$	$0.03^{0.00}_{0.00}$	0.00	True